Single-Step Synthesis, Characterization, and Application of Nanostructured $K_xMn_{1-y}Co_yO_{2-\delta}$ with Controllable Chemical Compositions and Crystal Structures

Sun Hee Lee, Tae Woo Kim, Dae Hoon Park, Jin-Ho Choy, and Seong-Ju Hwang*

Center of Intelligent Nano-Bio Materials (CINBM), Division of Nano Sciences and Department of Chemistry, Ewha Womans University, Seoul 120-750, Korea

Nanzhe Jiang and Sang-Eon Park

Department of Chemistry, Inha University, Incheon 700-742, Korea

Young-Ho Lee

Korea Institute of Ceramic Engineering and Technology, Seoul 153-801, Korea

Received March 6, 2007. Revised Manuscript Received July 23, 2007

Cobalt-substituted manganese oxide one-dimensional (1D) nanowires have been synthesized through one-pot hydrothermal treatment of the ion pair solution of Co^{2+} and MnO_4^-, along with their three-dimensional (3D) hierarchically assembled microspheres. The stabilization of cobalt ion in the manganese sites of α- and δ-MnO_2 structures was clearly evidenced by Mn K-edge and Co K-edge X-ray absorption spectroscopy as well as by powder X-ray diffraction and elemental analyses. The chemical composition, crystal structure, and morphology of the resultant nanostructures can be easily tailored through the control of reaction condition and precursor composition. That is, 1D nanowires with the tunnel-type α-MnO_2 structure can be prepared by the reaction at 140 °C, whereas the lowering of reaction temperature or the increase of Co content gives rise to the synthesis of 3D hierarchical nanostructured microspheres with the layered δ-MnO_2 structure. It has been obviously demonstrated that the partial Co substitution for the nanostructured manganese oxides causes the improvement of their catalytic activity with respect to olefin oxidation as well as affects significantly their electrode performances. The present study provides an effective way of controlling the chemical properties and functionalities of nanostructured manganese oxides through cation substitution.

Introduction

Over the past decade, intense research efforts have been devoted on the synthesis and characterization of nanostructured materials since the fabrication of low-dimensional nanostructures leads to the creation of unique and unexpected properties even from well-known materials like Au quantum dots.[1,2] Such intriguing effects of nanostructure formation have also been well-known for metal oxides.[1,2] Among various transition metal oxides, manganese oxides have attracted much attention because of their wide applications as electrodes for Li^+ ion batteries, redox catalysts, and absorbents.[3−8] On the basis of the expectation that their functionalities can be improved through the fabrication of nanostructures, several attempts have been made to synthesize one-dimensional (1D) nanostructured manganese oxides and their three-dimensional (3D) assembly of hierarchical superstructures.[3−6,9−11] In addition to the architecturing of

* To whom correspondence should be addressed. Tel.: +82-2-3277-4370. Fax: +82-2-3277-3419. E-mail: hwangsju@ewha.ac.kr.

(1) (a) Nalwa, H. S., Ed. *Encyclopedia of Nanoscience and Nanotechnology*; American Scientific Publishers: Stevenson Ranch, CA, 2004. (b) Schwarz, J. A., Contescu, C. I., Putyera, K., Eds. *Dekker Encyclopedia of Nanoscience and Nanotechnology*; Marcel Dekker Inc.: New York, 2004 and references therein.

(2) (a) Dai, H.; Wong, E. W.; Lu, Y. Z.; Fan, S.; Lieber, C. M. *Nature* **1995**, *375*, 769. (b) Xia, Y.; Yang, P.; Sun, Y.; Wu, Y.; Mayers, B.; Gates, B.; Yin, Y.; Kim, F.; Yan, H. *Adv. Mater.* **2003**, *15*, 353 and references therein.

(3) (a) Ma, R.; Bando, Y.; Zang, L.; Sasaki, T. *Adv. Mater.* **2004**, *16*, 918. (b) Subramanian, V.; Zhu, H.; Vajtai, R.; Ajayan, P. M.; Wei, B. *J. Phys. Chem. B* **2005**, *109*, 20207.

(4) (a) Chen, X.; Li, X.; Jiang, Y.; Shi, C.; Li, X. *Solid State Commun.* **2005**, *136*, 94. (b) Zhang, G.-Q.; Bao, S.-J.; Zhang, X.-G.; Li, H.-L. *J. Solid State Electrochem.* **2005**, *9*, 655.

(5) (a) Li, W.-N.; Yuan, J.; Shen, X.-F.; Gomez-Mower, S.; Xu, L. P.; Sithambaram, S.; Aindow, M.; Suib, S. L. *Adv. Funct. Mater.* **2006**, *16*, 1247. (b) Shen, X. F.; Ding, Y. S.; Liu, J.; Cai, J.; Laubernds, K.; Zerger, R. P.; Vasiliev, A.; Aindow, M.; Suib, S. L. *Adv. Mater.* **2005**, *7*, 805.

(6) (a) Ding, Y.-S.; Shen, X.-F.; Gomez, S.; Luo, H.; Aindow, M.; Suib, S. L. *Adv. Funct. Mater.* **2006**, *16*, 549. (b) Yuan, J.; Li, W. N.; Gomez, S.; Suib, S. L. *J. Am. Chem. Soc.* **2005**, *127*, 14184 and references therein.

(7) Thackeray, M. M. *Prog. Solid State Chem.* **1997**, *25*, 1 and references therein.

(8) (a) Kim, J.; Manthiram, A. *Nature* **1997**, *390*, 265. (b) Poizot, P.; Laruelle, S.; Grugeon, S.; Dupont, L.; Tarascon, J. M. *Nature* **2000**, *407*, 496 and references therein.

(9) (a) Benaissa, M.; Jose-Yacaman, M.; Xiao, T. D.; Strutt, P. R. *Appl. Phys. Lett.* **1997**, *70*, 2120. (b) Chitrakar, R.; Kanoh, H.; Kim, Y. S.; Miyai, Y.; Ooi, K. *J. Solid State Chem.* **2001**, *160*, 69. (c) Xiao, T. D.; Strutt, P. R.; Benaisd, M.; Chen, H.; Keart, B. H. *Nanostruct. Mater.* **1998**, *10*, 1051.

(10) Wang, X.; Li, Y. *J. Am. Chem. Soc.* **2002**, *124*, 2880.

(11) (a) Wang, X.; Li, Y. *Chem. Commun.* **2002**, 764. (b) Wang, X.; Li, Y. *Chem. Eur. J.* **2003**, *9*, 300.

10.1021/cm070633d CCC: $37.00
Published on Web 09/07/2007

nanostructure, the control of chemical composition and crystal structure can provide an effective tool for optimizing the physicochemical properties of the metal oxide. However, there have been only a few examples of the 1D nanostructure of cation-substituted manganese oxide.[12,13] Recently we have invented a hydrothermal method with solid-state precursor, in which the chemical composition of the resultant 1D nanowire of the metal oxide is controllable by changing the chemical formula of the precursor.[12] But the use of solid-state precursor prepared at elevated temperature of >900 °C is rather problematic from the viewpoint of energy consumption. Moreover, a requirement of multistep synthetic processes is not suitable for the mass production of nanomaterials. Very recently, Ding et al. have reported hydrothermal synthesis of the urchin-like 3D nanostructure of chromium-substituted manganese oxide.[6a] Although it is very crucial to assemble the low-dimensional nanostructured materials in the form of a 3D superstructure, the synthesis of individual 1D nanostructured metal oxides is of special importance for their applications as interconnects and active components in nanoscale devices. Even though Fe doping for α-MnO_2-type manganate nanofibers has been achieved via multistep solid-state reaction at elevated temperature,[13] there have been no reports on one-pot soft chemical synthesis of cation-substituted manganese oxide nanowires.

Here we report single-step hydrothermal synthesis and characterization of quaternary $K_xMn_{1-y}Co_yO_{2-\delta}$ 1D nanowires and their 3D hierarchical assemblies. With this method, the nanostructured materials can be prepared at a low temperature of <140 °C via the hydrothermal treatment of the ion pair solution of MnO_4^- and Co^{2+}. Moreover, we are able to easily control the chemical composition, crystal structure, and morphology of the resultant nanostructures through the change of reaction condition and precursor composition. Also, their catalytic activity for olefin oxidation as well as their electrode performance for lithium secondary batteries has been investigated.

Experimental Section

Sample Preparation. Nanostructured $K_xMn_{1-y}Co_yO_{2-\delta}$ samples were prepared by a hydrothermal reaction for the aqueous solution of $KMnO_4$, $CoSO_4$, and $(NH_4)_2S_2O_8$ at 100 and 140 °C for 12 h. The ratio of Co/Mn was varied from 1:10 to 1:2. The obtained powders were washed thoroughly with distilled water and dried at 50 °C in air. Typically several grams of the nanostructured materials could be easily obtained for each batch.

Sample Characterization. The crystal structures of the nanostructured cobalt manganese oxides were studied by powder X-ray diffraction (XRD) measurement using Ni-filtered Cu Kα radiation with a graphite diffracted beam monochromator. Their chemical compositions were determined using inductively coupled plasma (ICP) spectrometry. The thermal behaviors of the nanostructured materials were examined by performing thermogravimetric analysis (TGA) under Ar atmosphere at the rate of 10 °C/min. The crystallite morphology and cation composition of the $K_xMn_{1-y}Co_yO_{2-\delta}$ samples were probed by field emission scanning electron microscopy (FE-SEM)/energy-dispersive spectrometry (EDS) with a Jeol JSM-6700F microscope equipped with an energy-dispersive X-ray spectrometer). The crystal dimension and crystal symmetry of the present materials were examined by performing high-resolution transmission electron microscopy (HR-TEM)/selected area electron diffraction (SAED) measurement with a Philips-CM200 microscope at an accelerating voltage of 200 kV. Their surface area and porosity were examined by measuring volumetrically nitrogen adsorption−desorption isotherms at liquid nitrogen temperature. The samples were degassed at 100 °C for 2 h under vacuum prior to the adsorption measurement. X-ray absorption spectroscopy (XAS) experiments were carried out at the Mn and Co K-edges using an extended X-ray absorption fine structure (EXAFS) facility installed at the beam line 7C at the Pohang Accelerator Laboratory (PAL) in Pohang, Korea. The XAS measurements were done at room temperature in a transmission mode using gas-ionization detectors. All the present spectra were calibrated by measuring the spectrum of Mn or Co metal foil. The data analysis for the experimental spectra was performed by the standard procedure reported previously.[14,15] In the course of the EXAFS fitting analysis, all the coordination numbers (CN) were fixed to the crystallographic values while the amplitude reduction factor (S_0^2) was allowed to vary. The best-fit S_0^2's of all the present materials are consistent with one another within 20% deviation. All the bond distances (R), Debye−Waller factors (σ^2), and energy shifts (ΔE) were set as variables. In the case of α-MnO_2-structured materials, the energy shifts were kept the same for two adjacent (Mn/Co−Mn/Co) shells. This can be rationalized from the fact that the adjacent shells consisting of the same types of atoms at very close distances would possess nearly the same degree of energy shift and structural disorder.[14]

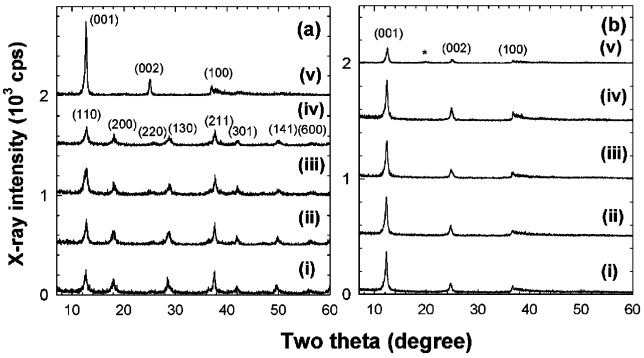

Figure 1. Powder XRD patterns for nanostructured $K_xMn_{1-y}Co_yO_{2-\delta}$ prepared at (a) 140 and (b) 100 °C with the Co/Mn ratios in the precursor of (i) 1/10, (ii) 1/8, (iii) 1/6, (iv) 1/4, and (v) 1/2. The asterisk represents the impurity $Co(OH)_2$ phase.

Catalytic Activity Test. The catalytic activity of the nanostructured $K_xMn_{1-y}Co_yO_{2-\delta}$ materials was tested for the oxidation of cyclohexene. A typical reaction was carried out with the reaction mixture of 50 mg of catalyst, 5 mmol of olefinic substrate, 5 mmol of *tert*-butyl hydrogen peroxide (TBHP), and 15 mL of acetonitrile solvent. All the reactions were performed at 60 °C for 24 h in open atmosphere under magnetic stirring. For all product analysis, mesitylene was used as an internal standard. Gas chromatography−mass spectrometry (GC−MS) was utilized for the identification and the quantification of the reaction products.

Electrochemical Property Measurement. The electrochemical measurements were performed with the cell of Li/1 M $LiPF_6$ in an

(12) Park, D. H.; Lim, S. T.; Hwang, S.-J.; Yoon, C.-S.; Sun, Y. K.; Choy, J. H. *Adv. Mater.* **2005**, *17*, 2834.
(13) (a) Liu, J.; Son, Y.-C.; Cai, J.; Shen, X.; Suib, S. L.; Aindow, M. *Chem. Mater.* **2004**, *16*, 276. (b) Cai, J.; Liu, J.; Willis, W. S.; Suib, S. L. *Chem. Mater.* **2001**, *13*, 2413.
(14) Teo, B. K. *EXAFS: Basic Principles and Data Analysis*; Springer-Verlag: Berlin, 1986.
(15) Choy, J.-H.; Hwang, S.-J.; Park, N. G. *J. Am. Chem. Soc.* **1997**, *117*, 1654.

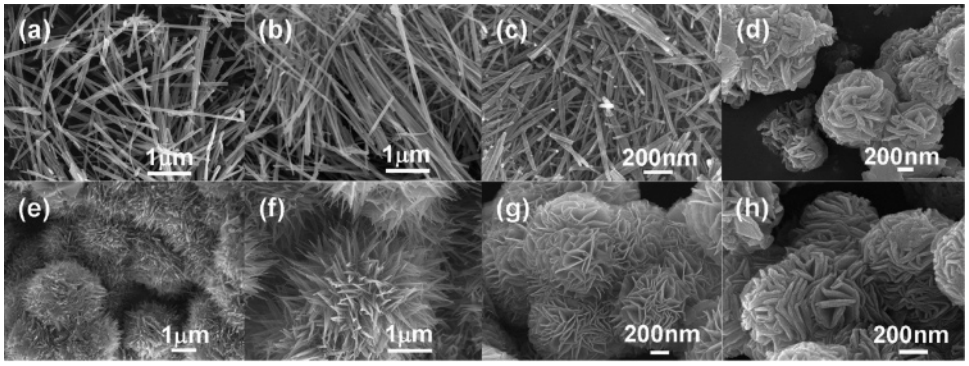

Figure 2. FE-SEM images from nanostructured $K_xMn_{1-y}Co_yO_{2-\delta}$ prepared at 140 °C with the Co/Mn ratios of (a) 1/10, (b) 1/8, (c) 1/4, and (d) 1/2, and (e−h) the corresponding data for the samples prepared at 100 °C.

Table 1. Lattice Parameters *a* and *c*, Crystal Symmetry, Oxygen Defect, Co/Mn and K/Mn Ratios, Water Content, and Surface Area (S_{BET}) of the Nanostructured $K_xMn_{1-y}Co_yO_{2-\delta}$ Compounds

sample	*a* (Å)	*c* (Å)	crystal symmetry	oxygen defect (δ)	Co/Mn ratio[a]	K/Mn ratio[a]	water content	S_{BET} ($m^2\ g^{-1}$)
			$K_xMn_{1-y}Co_yO_{2-\delta}$ prepared at 140 °C					
Co/Mn(1/10)	9.949(9)	2.852(2)	tetragonal	0.25	0.10	0.11	0.11	143
Co/Mn(1/8)	9.941(9)	2.854(5)	tetragonal	0.24	0.11	0.10	0.12	144
Co/Mn(1/6)	9.945(1)	2.850(1)	tetragonal	0.25	0.15	0.09	0.13	142
Co/Mn(1/4)	9.949(9)	2.852(2)	tetragonal	0.22	0.16	0.08	0.15	138
Co/Mn(1/2)	2.841(1)	7.216(1)	hexagonal	0.30	0.35	0.04	0.57	102
			$K_xMn_{1-y}Co_yO_{2-\delta}$ prepared at 100 °C					
Co/Mn(1/10)	2.743(4)	7.194(1)	hexagonal	0.36	0.11	0.09	0.57	70
Co/Mn(1/8)	2.741(1)	7.216(1)	hexagonal	0.39	0.14	0.07	0.55	76
Co/Mn(1/6)	2.743(1)	7.211(1)	hexagonal	0.37	0.20	0.06	0.53	72
Co/Mn(1/4)	2.740(1)	7.214(1)	hexagonal	0.35	0.27	0.05	0.46	86

[a] The ratios between metal components were determined by ICP analysis.

EC/DEC (ethylene carbonate/diethyl carbonate) (50:50 v/v)/ composite cathode, which was assembled in a drybox. The composite cathode was prepared by mixing thoroughly the active $K_xMn_{1-y}Co_yO_{2-\delta}$ material (62.5%) with 25% acetylene black and 12.5% PTFE (polytetrafluoroethylene). All the experiments were carried out in a galvanostatic mode with a Maccor multichannel galvanostat/potentiostat in the voltage range of 1.0−4.3 V at a constant current density 20 mA/g.

Results and Discussion

Powder XRD Analysis. Figure 1 represents the powder XRD patterns of nanostructured $K_xMn_{1-y}Co_yO_{2-\delta}$ prepared at 140 and 100 °C with various ratios of Co/Mn in the precursor solutions. A reaction at 140 °C with Co/Mn ratio of 1/10 to 1/4 produces the α-MnO_2-type structure, in which corner and edge-sharings of MnO_6 octahedra create 2 × 2 pores.[16] With higher Co content (i.e., Co/Mn ≥ 1/2), δ-MnO_2-structured materials composed of layered MnO_2 sheets accommodating water bilayers are formed,[16] indicating that the higher content of cobalt prefers this layered structure compared to the α-MnO_2 one.

On the other hand, at the lower temperature of 100 °C, the layered δ-MnO_2-type materials are obtained for the entire Co/Mn range applied here, but a weak impurity peak of $Co(OH)_2$ appears for the highest Co/Mn ratio of 1/2. The lattice parameters *a* and *c* of the present nanostructured materials were determined by Rietveld analyses with the help of the UWXAFS program, as listed in Table 1. These factors do not show monotonous and distinct dependencies on the ratio of Co/Mn, since there are many factors affecting the lattice parameters like water content, oxygen defect, relative ionic size of substitutents, etc. Moreover, the very similar sizes of Co^{4+} and Mn^{4+} ions and of Co^{3+} and Mn^{3+} ions contribute to the observed weak dependence of the lattice parameters on the Co content.[17]

FE-SEM and HR-TEM Analyses. As illustrated in Figure 2, FE-SEM analysis clearly demonstrates the formation of 1D nanowires through the hydrothermal reaction at 140 °C with the Co/Mn ratio of 1/10 to 1/4. The obtained nanowires possess diameters of about 20−30 nm and lengths of longer than 1 μm. The formation efficiency of the present nanowires is higher than 95%. At the highest ratio of 1/2, 3D hierarchical microspheres consisting of 2D nanoplates are obtained. The thickness of the component 2D nanoplates is about 50 nm. On the other hand, for the entire composition range, a reaction at 100 °C gives rise to the formation of 3D nanostructured microspheres with the radius of ∼1−2 μm, instead of well-separated 1D nanowires.

As shown in Figure 2, the microspheres prepared from the precursor with Co/Mn ≥ 1/4 consist of 2D nanoplates with the thickness of 10−20 nm, whereas the microspheres with the lower Co/Mn ratios are composed of needle-like 1D nanocrystallites. Very recently similar 3D assembled microspheres consisting of nanoneedles were reported for several MnO_2 polymorphs.[6a]

The crystal structure and crystallite dimension of 1D nanostructured materials were also probed with HR-TEM/

(16) Wells, A.-F. *Structural Inorganic Chemistry*; Clarendon Press: Oxford, 1984.

(17) Shannon, R. D. *Acta. Crystallogr., Sect. A* **1976**, *32*, 751.

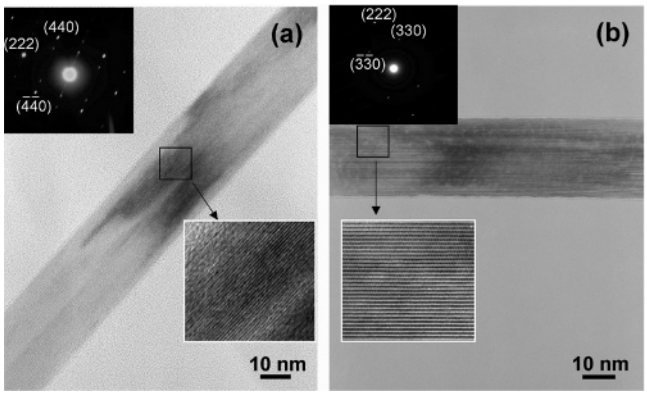

Figure 3. HR-TEM bright-field images and SAED patterns of the 1D nanowire of α-MnO_2-type $K_xMn_{1-y}Co_yO_{2-\delta}$ with the Co/Mn ratios of (a) 1/10 and (b) 1/4.

SAED analyses. As presented in Figure 3, the formation of single-crystalline 1D nanowires is evidenced from the observation of well-aligned lattice lines in the HR-TEM images. The dimensions of the nanostructures are in good agreement with the estimated values from the FE-SEM results. The SAED patterns of the present nanowires coincide well with the α-MnO_2-structure, attesting to the single-crystalline nature of the individual nanowires. From the HR-TEM/SAED analyses, the growth direction of the nanowires was determined as the [111] direction.

TG−DTA, Elemental, and N_2 Adsorption−Desorption Isotherm Measurements. According to ICP and EDS results, all of the present compounds surely contain both Co and Mn ions in the Co/Mn ratio of 0.10−0.16 for the α-MnO_2-type materials and 0.11−0.35 for the δ-MnO_2-type ones. This result underscores that the cobalt-substituted manganese oxide nanostructures were successfully prepared by the hydrothermal treatment for the mixed solution of MnO_4^- and Co^{2+} ions at 100−140 °C. Such successful substitution of cobalt ions for manganese ions in the present nanostructures is believed to originate from the formation of ion pairs between permanganate anions and cobalt cations in the precursor solution. In the course of the crystal growth of the nanostructures, an electrostatic interaction between two differently charged ions makes possible the incorporation of cobalt ion into the manganate lattice. In fact, we found that a hydrothermal treatment for an aqueous solution of Mn^{2+} and Co^{2+} cations with the same charge gives unsubstituted binary MnO_2 nanowires. Moreover, the present method allows us to control the ratio of Co/Mn through the change of precursor composition, as presented in Table 1. In comparison with the α-MnO_2-type materials consisting of edge- and corner-shared octahedra,[16] the δ-MnO_2-structured compounds with edge-shared octahedra only can accommodate larger amount of cobalt ions, strongly suggesting more effective stabilization of Co ions in this layered structure. This conclusion is well consistent with the fact that many cobalt oxides or cobalt hydroxides crystallize with an edge-shared network of CoO_6 octahedra, rather than a corner-shared one.[16] All the present materials contain a small amount of potassium ions with ∼0.03−0.11 per unit formula. Such a low content of alkali metal in the nanowires is in good agreement with the previous report showing that the introduction of a small amount of sodium ions (Na/Mn < 0.5) leads to the formation of 1D nanowires.[18]

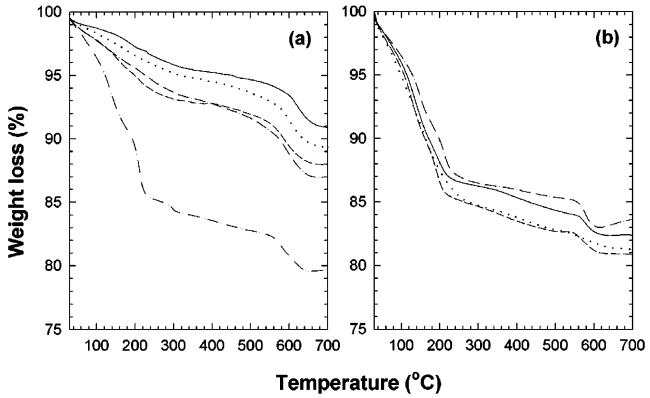

Figure 4. TGA curves of nanostructured $K_xMn_{1-y}Co_yO_{2-\delta}$ prepared at (a) 140 and (b) 100 °C with the Co/Mn ratios of 1/10 (solid lines), 1/8 (dotted lines), 1/6 (dashed lines), 1/4 (dot−dashed lines), and 1/2 (dot−dot−dashed lines).

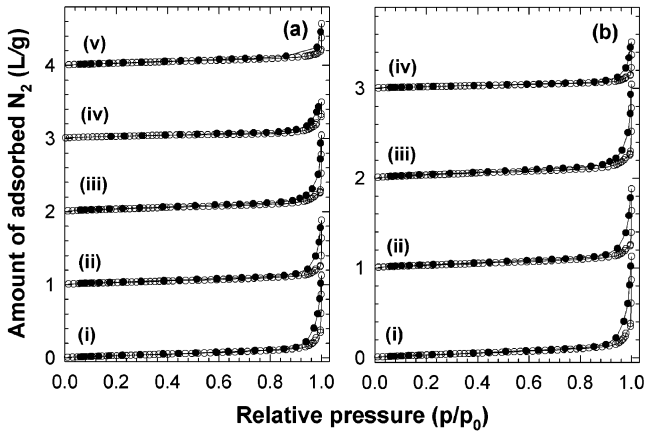

Figure 5. N_2 adsorption−desorption isotherms of nanostructured $K_xMn_{1-y}Co_yO_{2-\delta}$ prepared at (a) 140 and (b) 100 °C with the Co/Mn ratios of (i) 1/10, (ii) 1/8, (iii) 1/6, (iv) 1/4, and (v) 1/2.

Figure 4 represents the TGA data of the $K_xMn_{1-y}Co_yO_{2-\delta}$ nanostructures with Co/Mn ratios of 1/10 to 1/2. It is found that the δ-MnO_2- and α-MnO_2-type nanostructured manganese oxides show considerable weight losses of ∼5.0−6.2% and ∼1.7−2.7% in the temperature range of 100−250 °C, respectively, corresponding to the water content of 0.46−0.57 and 0.11−0.15 per unit formula. Due to the stabilization of the water bilayer in the interlayer space, the δ-MnO_2-structured materials show larger water content than the α-MnO_2-type compounds with 2 × 2 pores. A weight decrease corresponding to oxygen loss occurs at around 550−600 °C, resulting in the formation of a $(Mn,Co)_2O_3$ phase. Based on the amount of oxygen loss in this temperature range, we have calculated the oxygen content of the present materials, as listed in Table 1. The α-MnO_2-type materials possess higher oxygen contents than δ-MnO_2-type materials, implying the higher oxidation states of Mn and Co ions in the former.

Nitrogen adsorption−desorption isotherms of the $K_xMn_{1-y}Co_yO_{2-\delta}$ nanostructures are plotted in Figure 5. The present nanostructured materials show a weak hysteresis in the p/p_0 >

(18) Eftekhari, A.; Kazemzad, M.; Moztarzadeh, F. *Mater. Res. Bull.* **2005**, *40*, 2205.

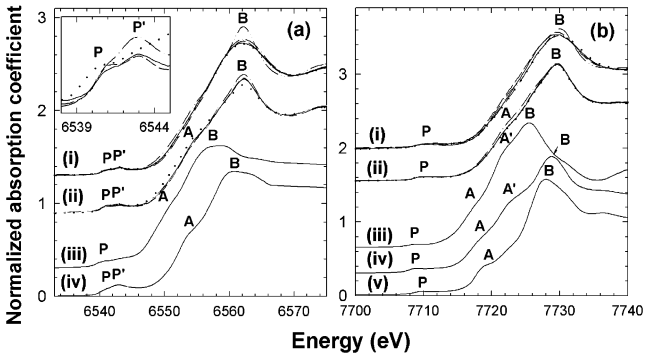

Figure 6. (a) Mn K-edge and (b) Co K-edge XANES spectra for nanostructured $K_xMn_{1-y}Co_yO_{2-\delta}$ synthesized at (i) 140 and (ii) 100 °C, (iii) Mn_2O_3/CoO, (iv) MnO_2/Co_3O_4, (v) $LiCoO_2$. In (i and ii), the data with the Co/Mn ratios of 1/10 (solid lines), 1/8 (dotted lines), 1/6 (dashed lines), 1/4 (dot−dashed lines), and 1/2 (dot−dot−dashed lines) are compared with one another. The inset presents the expanded views for the preedge region of 6538−6545 eV for $K_xMn_{1-y}Co_yO_{2-\delta}$ with the Co/Mn ratio of 1/10 synthesized at 140 (solid lines) and 100 °C (dashed lines), Mn_2O_3 (dotted lines), and MnO_2 (dot−dashed lines).

0.9 region, indicating the formation of mesopores due to the porous stacking of nanostructured crystallites.[19] According to pore size analysis based on the BJH (Barrett-Joyner-Halenda) method (see the Supporting Information), the δ-MnO_2-structured microspheres exhibit mesopores with the average diameters of 4.6−5.0 nm, while no distinct peak can be observed in the pore size distribution curves of the α-MnO_2-structured nanowires, suggesting nonuniform pore size distribution in these nanowires. A negligible adsorption of nitrogen in the low p/p_0 region clearly demonstrates the absence of micropores in the present materials. As listed in Table 1, the present materials have the expanded surface area of ∼102−144 m^2/g for the nanowires and ∼70−86 m^2/g for the nanostructured microspheres, respectively. The enhancement of surface area underscores the overall formation of nanostructured materials. The larger surface area of the nanowires compared to the microspheres is attributable to their nonaggregated morphology.

Mn K-Edge and Co K-Edge XANES Analyses. We have examined the chemical bonding nature of transition metal ions in the present nanostructures using X-ray absorption near-edge structure (XANES) analysis at Mn and Co K-edges. The Mn K-edge and Co K-edge XANES spectra of the nanostructured $K_xMn_{1-y}Co_yO_{2-\delta}$ are illustrated in Figure 6, parts a and b, respectively, in comparison with those of several references. For the Mn K-edge, all the nanostructured materials show small preedge peaks P and/or P′ corresponding to the 1s → 3d transitions, clarifying the stabilization of Mn ions in the octahedral site.[20] Also, it has been well-known that the relative intensity of the peak P′ to the peak P is proportional to the oxidation state of manganese ion.[20] In fact, the reference $Mn_2{}^{3+}O_3$ displays only one feature P, whereas an additional peak P′ can be clearly observed at higher energy commonly for the nanostructured materials and the reference MnO_2. As can be seen clearly from the inset of Figure 6a, the intensity of higher energy peak P′ is weaker for $K_xMn_{1-y}Co_yO_{2-\delta}$ than for the reference $Mn^{4+}O_2$. Since a spectral weight of the peak P′ is proportional to the Mn oxidation state,[20] the observed weaker intensity of the peak P′ for the nanostructured $K_xMn_{1-y}Co_yO_{2-\delta}$ than $Mn^{4+}O_2$ implies the mixed oxidation state of Mn^{3+}/Mn^{4+} in these nanomaterials. In the main-edge region, a broad and diffusive resonance peak B appears at ∼6560 eV in the Mn K-edge spectra of α-MnO_2-structured $K_xMn_{1-y}Co_yO_{2-\delta}$ prepared at 140 °C, whereas this feature is sharper and stronger for the δ-MnO_2-structured compounds prepared at 100 °C. Since the intensity and sharpness of the peak B are proportional to the relative ratio of edge-sharing to corner-sharing of MnO_6 octahedra,[21] its spectral variation can provide strong evidence on the stabilization of Mn ions in the corresponding α- and δ-MnO_2 structures.

Like the Mn K-edge data, all of the present compounds exhibit a weak preedge feature P in the Co K-edge region (Figure 6b), indicative of the stabilization of Co ions in the octahedral sites. The energy of the preedge peak is slightly higher for the $K_xMn_{1-y}Co_yO_{2-\delta}$ compounds than for the reference $LiCo^{3+}O_2$, indicating the mixed oxidation state of Co^{3+}/Co^{4+}. In the main-edge region, the lowering of the reaction temperature leads to the sharpening and enhancement of the resonance peak B, as observed in the Mn K-edge region. This can be regarded as evidence of the similar local environment of cobalt ions to that of manganese ions. Of interest is that this peak B shows somewhat higher energy for the reference $Co_3{}^{2.67+}O_4$ than for the reference $LiCo^{3+}O_2$, in spite of the lower Co oxidation state in the former. This is due to the different local symmetry of cobalt ions in these compounds. The presence of tetragonal distortion around divalent cobalt ions in Co_3O_4 leads to the splitting of 4p orbitals into $4p_{x,y}$ and $4p_z$ orbitals, resulting in two peaks A′ and B in the XANES region. On the contrary, no peak splitting occurs for $LiCoO_2$ with regular octahedral geometry of Co^{3+} ions. For this reason, the energy of the peak B in the spectrum of $LiCoO_2$ should be compared with the average position of the peaks A′ and B in the spectrum of Co_3O_4. The observed order of these energies matches well with the Co oxidation states in these compounds.

Mn K-Edge and Co K-Edge EXAFS Analyses. The local atomic arrangement around transition metal ions has been probed quantitatively with EXAFS tools. The Fourier transforms (FTs) of k^3-weighted Mn K-edge and Co K-edge EXAFS spectra of the $K_xMn_{1-y}Co_yO_{2-\delta}$ nanomaterials are plotted in Figure 7, in comparison with those of spinel-structured $LiMn_2O_4$ and rocksalt-structured CoO. For both the edges, the α-MnO_2-structured material (i.e., Co/Mn(1/6)−140 °C) shows three FT peaks at ∼1.6, 2.6, and 3.1 Å, which are attributed to the (Mn/Co−O) shell and edge-shared and corner-shared (Mn/Co−Mn/Co) shells. On the other hand, as in the case of spinel $LiMn_2O_4$ consisting of edge-shared MnO_6 octahedra, the δ-MnO_2-structured material (i.e., Co/Mn(1/4)−100 °C) does not display the most distant FT peak of the corner-shared (Mn/Co−Mn/Co) shell, since this structure consists of edge-shared $(Mn,Co)O_6$ octahedra

(19) Gregg, S. J.; Sing, K. S. W. *Adsorption, Surface Area and Porosity*; Academic Press: London, 1982.
(20) (a) Hwang, S.-J.; Kwon, C. W.; Portier, J.; Campet, G.; Park, H. S.; Choy, J.-H.; Huong, P. V.; Yoshimura, M.; Kakihana, M. *J. Phys. Chem. B* **2002**, *106*, 4053. (b) Hwang, S.-J.; Choy, J.-H. *J. Phys. Chem. B* **2003**, *107*, 5791.
(21) Manceau, A.; Gorshkov, A. I.; Drits, V. A. *Am. Mineral.* **1992**, *77*, 1133.

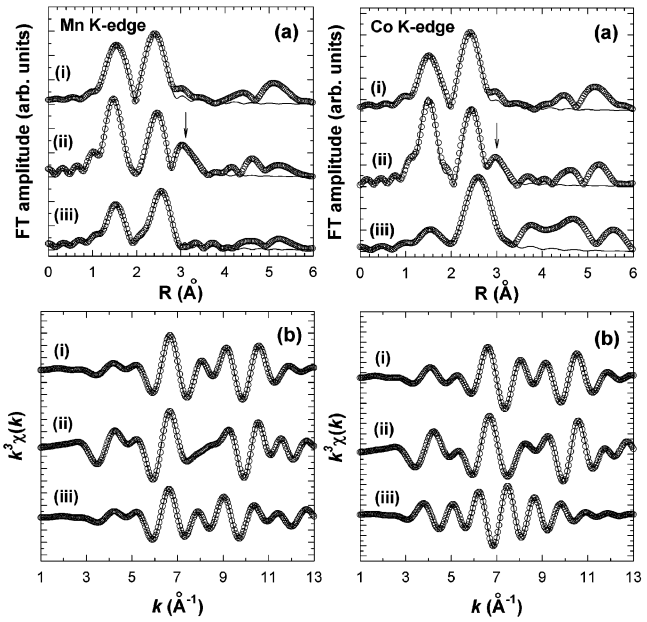

Figure 7. Mn K-edge (left panel) and Co K-edge (right panel) (a) FT and (b) Fourier-filtered EXAFS data for nanostructured $K_xMn_{1-y}Co_yO_{2-\delta}$ synthesized at (i) 100 and (ii) 140 °C and (iii) $LiMn_2O_4$/CoO. The arrows denote the FT peak corresponding to corner-shared (Mn/Co−Mn/Co) shell.

only.[16] The observation of similar FT features for the both Mn K-edge and Co K-edge data of the nanostructured materials can provide clear evidence on the stabilization of the substituent cobalt ion in the manganese sites of the crystal structures (i.e., α-MnO_2-and δ-MnO_2-structures).

In order to quantitatively determine the local structural parameters, the FT peaks were inversely Fourier-transformed to *k* space and curve-fitted. As presented in Figure 7, the reference spectra of $LiMn_2O_4$ and CoO could be well fitted with spinel and rocksalt structures, respectively. The best fits gave reasonable structural parameters for each compound, verifying the reliability of the present fitting analyses. On the other hand, all the present Mn K-edge and Co K-edge EXAFS spectra of the $K_xMn_{1-y}Co_yO_{2-\delta}$ nanomaterials are quite reproducible with the models of α-MnO_2- and δ-MnO_2-type structures.[22] As summarized in Tables 2 and 3, the fitting analyses gave reasonable structural parameters for each crystal structure. The metal ions in the δ-MnO_2-structured compounds are coordinated by six oxygen ligands at 1.91 Å and six metal ions at 2.82−2.84 Å, whereas there are three types of neighbors around metal ions in the α-MnO_2-structured compounds, i.e., six oxygen ligands at ∼1.89 Å, four metal neighbors at 2.83−2.86 Å, and four metal neighbors at 3.42−3.44 Å. The bond distances of metal−oxygen pairs are nearly identical for both the cobalt and manganese ions, confirming their existence in the same crystal sites. A comparison with the reference data reveals that the (Mn−O) bond distances for the $K_xMn_{1-y}Co_yO_{2-\delta}$ materials are nearly identical to that for the reference $LiMn_2^{3.5+}O_4$, confirming similar Mn oxidation states in these compounds. On the contrary, the $K_xMn_{1-y}Co_yO_{2-\delta}$ compounds show much shorter (Co−O) bond distances than the reference $Co^{2+}O$, underscoring the higher Co oxidation state in the former.

Table 2. Results of Curve-Fitting Analysis for the Mn K-Edge EXAFS Spectra

sample	bond	CN	*R* (Å)	σ^2 ($10^{-3}\times$ Å^2)
Co/Mn(1/4)−100 °C[a]	(Mn−O)	6.0	1.91	1.81
	$(Mn-Mn/Co)_{edge}$	6.0	2.84	3.37
Co/Mn(1/6)−140 °C[b]	(Mn−O)	6.0	1.89	3.07
	$(Mn-Mn/Co)_{edge}$	4.0	2.86	3.71
	$(Mn-Mn/Co)_{corner}$	4.0	3.44	5.08
$LiMn_2O_4$[c]	(Mn−O)	6.0	1.90	4.30
	(Mn−Mn)	6.0	2.91	4.82

[a] The curve-fitting analysis was performed for 1.012−*R*−2.823 Å and 3.75−*k*−11.65 Å^{-1}. [b] The curve-fitting analysis was performed for 0.92−*R*−3.528 Å and 2.85−*k*−12.4 Å^{-1}. [c] The curve-fitting analysis was performed for 0.982−*R*−2.976 Å and 3.8−*k*−13.0 Å^{-1}.

Table 3. Results of Curve-Fitting Analysis for the Co K-Edge EXAFS Spectra

sample	bond	CN	*R* (Å)	σ^2 ($10^{-3}\times$ Å^2)
Co/Mn(1/4)−100 °C[a]	(Co−O)	6.0	1.91	2.72
	$(Co-Mn/Co)_{edge}$	6.0	2.82	3.19
Co/Mn(1/6)−140 °C[b]	(Co−O)	6.0	1.89	2.38
	$(Co-Mn/Co)_{edge}$	4.0	2.83	2.75
	$(Co-Mn/Co)_{corner}$	4.0	3.42	8.24
CoO[c]	(Co−O)	6.0	1.97	11.17
	(Co−Co)	12.0	2.99	8.38

[a] The curve-fitting analysis was performed for 1.043−*R*−2.823 Å and 3.65−*k*−11.5 Å^{-1}. [b] The curve-fitting analysis was performed for 0.982−*R*−3.375 Å and 2.55−*k*−12.3 Å^{-1}. [c] The curve-fitting analysis was performed for 1.135−*R*−3.037 Å and 3.4−*k*−10.0 Å^{-1}.

As listed in Tables 2 and 3, the Debye−Waller factor (σ^2) reflecting the degree of structural disorder exhibits only a small difference for a specific bonding pair between Mn K-edge and Co K-edge data, confirming the similar local atomic environment between manganese and cobalt ions. Summarizing the XANES/EXAFS results presented here, it is certain that both the Mn and Co ions exist in the same octahedral sites of α-MnO_2- and δ-MnO_2-type structures.

Catalytic Tests for Olefin Oxidation. The catalytic activity of the nanostructured $K_xMn_{1-y}Co_yO_{2-\delta}$ materials has been examined with respect to the oxidation of cyclohexene. With the presence of these nanomaterials, the substrate cyclohexene can be oxidized to alcohol or ketone through the oxidation at the allyl position. In addition, a small amount of polymeric byproducts was detected, suggestive of the formation of an intermediate allyl radical through the dehydrogenation of cyclohexene.[23,24] The dominant product of the reaction is 2-cyclohexen-1-one with the relatively high selectivity of ∼61−75%.

As summarized in Table 4, the $K_xMn_{1-y}Co_yO_{2-\delta}$ compounds with higher Co/Mn ratio show better catalytic activity

(22) The best-fits to the experimental EXAFS data gave the residual F^2 factor ($= \sum\{k_3(\chi(k)_{cal} - \chi(k)_{exp})\}^2/(n-1)$, *n* is the number of data) as follows: $K_xMn_{1-y}Co_yO_{2-\delta}$ synthesized at 100 °C, 0.066 (Mn K-edge), 0.061 (Co K-edge); $K_xMn_{1-y}Co_yO_{2-\delta}$ synthesized at 140 °C, 0.232 (Mn K-edge), 0.178 (Co K-edge); $LiMn_2O_4$, 0.077 (Mn K-edge); CoO, 0.033 (Co K-edge).

(23) (a) Shen, X.; Ding, Y.; Liu, J.; Laubernds, K.; Zerger, R. P.; Polverejan, M.; Son, Y.-C.; Aindow, M.; Suib, S. L. *Chem. Mater.* **2004**, *16*, 5327. (b) Ghosh, R.; Son, Y.-C.; Suib, S. L. *J. Catal.* **2004**, *224*, 288.
(24) (a) Xia, G. G.; Yin, Y. G.; Willis, W. S.; Wang, J. Y.; Suib, S. L. *J. Catal.* **1999**, *185*, 91. (b) Luo, R.; Zhang, Q.; Huang, A.; Suib, S. L. *Microporous Mesoporous Mater.* **2000**, *35*−*36*, 209.

Table 4. Results of Cyclohexene Oxidation Catalyzed by Nanostructured $K_xMn_{1-y}Co_yO_{2-\delta}$ Compounds

		selectivity (%)		
sample	conversion (%)	2-cyclohexen-1-ol	2-cyclohexen-1-one	polymeric byproducts
$K_xMn_{1-y}Co_yO_{2-\delta}$ prepared at 140 °C				
Co/Mn(1/10)	43.2	19.2	74.6	6.2
Co/Mn(1/4)	44.8	18.3	75.4	6.3
$K_xMn_{1-y}Co_yO_{2-\delta}$ prepared at 100 °C				
Co/Mn(1/10)	31.7	26.8	61.2	6.0
Co/Mn(1/4)	46.9	19.0	74.8	6.2

(i.e., higher conversion rate and higher selectivity) than the other samples with the same structure type and the lower Co/Mn ratio, underscoring the positive influence of cobalt substitution. Also, a comparison between the nanostructured samples with nearly the same Co content but with different structure type (i.e., the samples prepared at 100 and 140 °C with Co/Mn ratio of 1/10) clearly demonstrates that the α-MnO_2-structured material is more catalytically active than δ-MnO_2-structured material. This can be interpreted as a result of the larger surface area of the former (Table 1). Also, between these two samples, the δ-MnO_2-structured material was found to show a poor selectivity for 2-cyclohexen-1-one, which is mainly due to the production of a larger amount of alcohol species. This result would be related to the higher amount of lattice water in this material (Table 1), since the presence of water molecules can facilitate the formation of 2-cyclohexen-1-ol through the stabilization of the product via hydrogen bonding with water molecules. Also, we have measured the catalytic activity of the nanostructured material with the highest Co content, namely, 3D microsphere prepared at 100 °C with the Co/Mn ratio of 1/2. This material shows high activity but poor selectivity for the ketone (conversion rate, 56.6%; selectivity, 36.2%), suggesting that the Co substitution at a very high rate is not favorable for the production of 2-cyclohexen-1-one. In fact, a catalysis reaction of cyclohexene by cobalt oxide Co_3O_4 was found to produce 2-cyclohexen-1-ol as a main product (64.0%), instead of the 2-cyclohexen-1-one (19.2%). On the other hand, unsubstituted α-MnO_2 nanowire was also tested as a catalyst, revealing that this material exhibits poor selectivity for the formation of ketone (44.1%). Although this manganate nanowire seems to show a relatively higher conversion rate of 55% than the present $K_xMn_{1-y}Co_yO_{2-\delta}$ nanostructures, this high conversion of cyclohexene is just due to the formation of an intermediate adduct between cyclohexene and TBHP (i.e., 1-(*tert*-butylperoxy)-2-cyclohexene), not to that of 2-cyclohexen-1-one (i.e., the product of complete oxidation reaction). Therefore, the observed high conversion of cyclohexene by the pure α-MnO_2 nanowires does not imply its high catalytic activity. In fact, the production efficiency for the 2-cyclohexen-1-one is lower for the unsubstituted α-MnO_2 nanowires than for the present $K_xMn_{1-y}Co_yO_{2-\delta}$ nanostructures, highlighting that the partial substitution of Mn with Co improves the catalytic activity of nanostructured manganese oxide for the formation of 2-cyclohexen-1-one. Although the mechanism for the positive effect of Co substitution is not clear at present, this is believed to be due to the strong oxidation power of Co^{3+}/Co^{4+} ions, compared to Mn^{3+}/Mn^{4+} ions.

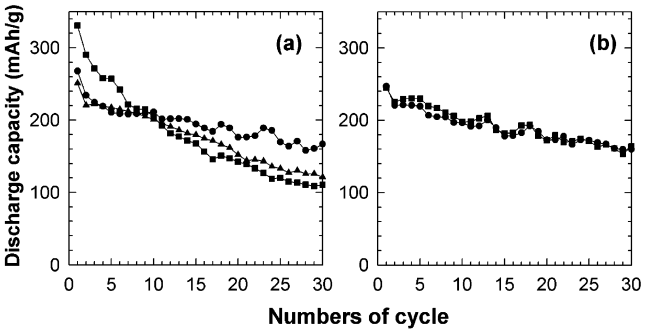

Figure 8. Variation of discharge capacity as a function of cycle number for nanostructured $K_xMn_{1-y}Co_yO_{2-\delta}$ with the Co/Mn ratios of 1/10 (circles) and 1/4 (squares) prepared at (a) 140 and (b) 100 °C, in comparison with α-MnO_2 nanowire (triangles).

Electrochemical Measurements. Judging from their crystal structures and metal oxidation states, the obtained nanostructured materials are expected to be applicable as an intercalation electrode for lithium secondary batteries. In this regard, we have carried out electrochemical measurements for their electrode performances over the potential range of 1.0−4.3 V. All of the present materials show smoother potential curves than the microcrystalline electrode material, which is characteristic of nanocrystalline metal oxide (see the Supporting Information).[8,20]

As plotted in Figure 8a, the α-MnO_2-type nanowire with the Co/Mn ratio of 1/10 shows better performance with good cyclability after the initial several cycles than the unsubstituted α-MnO_2 nanowire, highlighting the effectiveness of Co substitution in improving the electrode performance of manganese oxide nanowires. However, the further increase of cobalt concentration of Co/Mn ≥ 1/8 makes capacity fading severe although it leads to the increase of initial capacity. The present findings underscore that there is an optimal Co substitution rate for enhancing the electrochemical properties of nanostructured manganese oxide, as in the case of previously studied microcrystalline manganese oxides.[25] On the contrary, the δ-MnO_2-structured material with high Co/Mn = 1/4 exhibits much better cyclability than the α-MnO_2-type homologue. This observation strongly suggests that the cobalt ion possesses high stability in the layered δ-MnO_2-structure, whereas it becomes unstable within the α-MnO_2-structure. This is well consistent with the better ability of δ-MnO_2-structured materials to accommodate cobalt ions (Table 1).

Conclusion

We have successfully synthesized the 1D nanowires and their 3D hierarchically assembled microspheres of quaternary $K_xMn_{1-y}Co_yO_{2-\delta}$ via one-pot hydrothermal reaction at a low temperature of <140 °C without the use of a solid-state precursor prepared at elevated temperature. To the best of our knowledge, this is the first example of cation-substituted manganese oxide 1D nanowires synthesized by one-pot soft

(25) Armstrong, A. R.; Gitzendanner, R.; Robertson, A. D.; Bruce, P. G. *Chem. Commun.* **1998**, 1833.

chemical reaction. Using various spectroscopic tools, we have found that the mixed valent Co^{3+}/Co^{4+} ions are stabilized in the octahedral sites of α- and δ-MnO_2 structures, along with the mixed valent Mn^{3+}/Mn^{4+} ions. With the present method, one can easily control the cation composition, crystal structure, and crystallite morphology of the nanostructured metal oxides by changing the reactant ratio and reaction temperature. Of special importance is that the resultant cobalt manganese oxide nanostructures show promising performances as redox catalysts and intercalation electrodes. Our current project is the optimization of their catalytic activity with respect to diverse organic reactions.

Acknowledgment. This work was performed by the Korea Research Foundation Grant funded by the Korean Government (MOEHRD, Basic Research Promotion Fund) (KRF-2006-312-C00220) and partly by the SRC/ERC program of the MOST/KOSEF (Grant R11-2005-008-03002-0). The experiments at Pohang Accelerator Laboratory (PAL) were supported in part by MOST and POSTECH.

Supporting Information Available: Pore size distribution curves and discharge potential profiles of nanostructured $K_xMn_{1-y}Co_yO_{2-\delta}$ compounds (PDF). This material is available free of charge via the Internet at http://pubs.acs.org.

CM070633D